UNIVERSITY
OF TRENTO

DIPARTIMENTO DI INGEGNERIA E SCIENZA DELL'INFORMAZIONE

38123 Povo – Trento (Italy), Via Sommarive 14
http://www.disi.unitn.it

METAMATERIAL LENSES FOR ANTENNA ARRAYS CIRCULAR TO LINEAR ARRAY TRANSFORMATION

E. T. Bekele, F. Viani, L. Manica, Douglas H. Werner and A. Massa

March 2013

Technical Report # DISI-13-007

Contents

1 Introduction

This report presents the progress on activities carried out on the topic of Metamaterial lenses used in antenna arrays.

2 Mathematical Formulation

Each one step transformation involves two domains. In this report, the first domain is called "virtual domain" or "virtual space" while the other one is referred to as "physical domain" or "physical space". In addition, the terms "virtual" and "physical" are used to describe entities in virtual and physical spaces respectively. The rectangular coordinate system in virtual space is labeled as (x', y', z') whereas in the physical space the labels (x, y, z) are used.

If the transformation from (x', y', z') to (x, y, z) is defined as:

$$(x, y, z) = \Gamma\left(x', y', z'\right) \tag{1}$$

$$x = x\left(x', y', z'\right) \tag{2}$$

$$y = y\left(x', y', z'\right) \tag{3}$$

$$z = z\left(x', y', z'\right) \tag{4}$$

the Jacobian matrix of the transformation $\underline{\Lambda}$ will be:

$$\underline{\Lambda} = \begin{bmatrix} \frac{\partial x}{\partial x'} & \frac{\partial x}{\partial y'} & \frac{\partial x}{\partial z'} \\ \frac{\partial y}{\partial x'} & \frac{\partial y}{\partial y'} & \frac{\partial y}{\partial z'} \\ \frac{\partial z}{\partial x'} & \frac{\partial z}{\partial y'} & \frac{\partial z}{\partial z'} \end{bmatrix}. \tag{5}$$

For the inverse transformation i.e. (x, y, z) to (x', y', z'),

$$(x', y', z') = \Gamma'\left(x, y, z\right) \tag{6}$$

$$x' = x'\left(x, y, z\right) \tag{7}$$

$$y' = y'\left(x, y, z\right) \tag{8}$$

$$z' = z'\left(x, y, z\right) \tag{9}$$

the corresponding Jacobian matrix will be

$$\underline{\Lambda}' = \begin{bmatrix} \frac{\partial x'}{\partial x} & \frac{\partial x'}{\partial y} & \frac{\partial x'}{\partial z} \\ \frac{\partial y'}{\partial x} & \frac{\partial y'}{\partial y} & \frac{\partial y'}{\partial z} \\ \frac{\partial z'}{\partial x} & \frac{\partial z'}{\partial y} & \frac{\partial z'}{\partial z} \end{bmatrix}. \tag{10}$$

and the following relations can be established.

$$\underline{\Lambda}' = \underline{\Lambda}^{-1} \tag{11}$$

$$det\left(\underline{\Lambda}'\right) = \frac{1}{det\left(\underline{\Lambda}\right)} \tag{12}$$

If $\underline{\epsilon}'$ and $\underline{\mu}'$ represent permittivity and permeability tensors in virtual medium respectively,

$$\underline{\epsilon}' = \begin{bmatrix} \epsilon'_{xx} & \epsilon'_{xy} & \epsilon'_{xz} \\ \epsilon'_{yx} & \epsilon'_{yy} & \epsilon'_{yz} \\ \epsilon'_{zx} & \epsilon'_{zy} & \epsilon'_{zz} \end{bmatrix} \tag{13}$$

$$\underline{\mu}' = \begin{bmatrix} \mu'_{xx} & \mu'_{xy} & \mu'_{xz} \\ \mu'_{yx} & \mu'_{yy} & \mu'_{yz} \\ \mu'_{zx} & \mu'_{zy} & \mu'_{zz} \end{bmatrix} \tag{14}$$

corresponding permittivity and permeability tensors in physical space can be computed as follows:

$$\underline{\epsilon} = \frac{\underline{\Lambda}\,\underline{\epsilon}'\,\underline{\Lambda}^T}{det\left(\underline{\Lambda}\right)} \tag{15}$$

$$\underline{\mu} = \frac{\underline{\Lambda}\,\underline{\mu}'\,\underline{\Lambda}^T}{det\left(\underline{\Lambda}\right)}. \tag{16}$$

If there is a source with current I' and current density J' in virtual space its corresponding image in the physical space can be computed as [2]

$$J = \frac{\underline{\Lambda}\,J'}{det\left(\underline{\Lambda}\right)}. \tag{17}$$

$$I = I'. \tag{18}$$

For a cascade of transformations: $\underline{\hat{\Gamma}}\left\{(x'', y'', z'') \rightarrow (x', y', z')\right\}$ followed by $\underline{\tilde{\Gamma}}\left\{(x', y', z') \rightarrow (x, y, z)\right\}$, the overall transformation $\underline{\Gamma}\left\{(x'', y'', z'') \rightarrow (x, y, z)\right\}$ can be formulated as follows. In the following discussion, and in the remaining of this report, when dealing with cascade of transformations, the space defined by the coordinates (x', y', z') will be termed as the *Intermediate* space and objects defined in this space will be called intermediate objects. Let $\underline{\hat{\Lambda}}$ and $\underline{\tilde{\Lambda}}$ represent the Jacobian matrices of the transformations $\underline{\hat{\Gamma}}$ and $\underline{\tilde{\Gamma}}$ respectively defined as:

$$\underline{\hat{\Lambda}} = \begin{bmatrix} \frac{\partial x'}{\partial x''} & \frac{\partial x'}{\partial y''} & \frac{\partial x'}{\partial z''} \\ \frac{\partial y'}{\partial x''} & \frac{\partial y'}{\partial y''} & \frac{\partial y'}{\partial z''} \\ \frac{\partial z'}{\partial x''} & \frac{\partial z'}{\partial y''} & \frac{\partial z'}{\partial z''} \end{bmatrix} \tag{19}$$

$$\underline{\tilde{\Lambda}} = \begin{bmatrix} \frac{\partial x}{\partial x'} & \frac{\partial x}{\partial y'} & \frac{\partial x}{\partial z'} \\ \frac{\partial y}{\partial x'} & \frac{\partial y}{\partial y'} & \frac{\partial y}{\partial z'} \\ \frac{\partial z}{\partial x'} & \frac{\partial z}{\partial y'} & \frac{\partial z}{\partial z'} \end{bmatrix}. \tag{20}$$

Further more, let $\left\{\underline{\epsilon}'', \underline{\mu}''\right\}$, $\left\{\underline{\epsilon}', \underline{\mu}'\right\}$ and $\left\{\underline{\epsilon}, \mu\right\}$ represent sets of permittivity and permeability tensors in (x'', y'', z''), (x', y', z') and (x, y, z) spaces respectively, while the corresponding currents are represented as J'',

J' and J. Considering the transformation: $\underline{\tilde{\Gamma}}\{(x', y', z') \rightarrow (x, y, z)\}$, the following relations can be established:

$$\underline{\epsilon} = \frac{\underline{\tilde{\Lambda}}\,\underline{\epsilon}'\,\underline{\tilde{\Lambda}}^T}{det\left(\underline{\tilde{\Lambda}}\right)} \tag{21}$$

$$\underline{\mu} = \frac{\underline{\tilde{\Lambda}}\,\underline{\mu}'\,\underline{\tilde{\Lambda}}^T}{det\left(\underline{\tilde{\Lambda}}\right)} \tag{22}$$

and for the other transformation, $\underline{\hat{\Gamma}}\{(x'', y'', z'') \rightarrow (x', y', z')\}$,

$$\underline{\epsilon}' = \frac{\underline{\hat{\Lambda}}\,\underline{\epsilon}''\,\underline{\hat{\Lambda}}^T}{det\left(\underline{\hat{\Lambda}}\right)} \tag{23}$$

$$\underline{\mu}' = \frac{\underline{\hat{\Lambda}}\,\underline{\mu}''\,\underline{\hat{\Lambda}}^T}{det\left(\underline{\hat{\Lambda}}\right)}. \tag{24}$$

Substituting (23) and (24) in (21) and (22) respectively and rearranging terms gives the relationship between material properties for the overall transformation

$$\underline{\epsilon} = \frac{\left(\underline{\tilde{\Lambda}}\underline{\hat{\Lambda}}\right)\,\underline{\epsilon}''\,\left(\underline{\tilde{\Lambda}}\underline{\hat{\Lambda}}\right)^T}{det\left(\underline{\tilde{\Lambda}}\underline{\hat{\Lambda}}\right)} \tag{25}$$

$$\underline{\mu} = \frac{\left(\underline{\tilde{\Lambda}}\underline{\hat{\Lambda}}\right)\,\underline{\mu}''\,\left(\underline{\tilde{\Lambda}}\underline{\hat{\Lambda}}\right)^T}{det\left(\underline{\tilde{\Lambda}}\underline{\hat{\Lambda}}\right)}. \tag{26}$$

Following similar analysis, the current sources for the complete transformation can be related as:

$$J = \frac{\left(\underline{\tilde{\Lambda}}\underline{\hat{\Lambda}}\right)\,J''}{det\left(\underline{\tilde{\Lambda}}\underline{\hat{\Lambda}}\right)}. \tag{27}$$

$$I = I' = I''. \tag{28}$$

2.1 +qTo Library

The +qTo software library is a numerical implementation of 2D Transformation. It takes boundary contour of virtual space as input and generates grid of transformation to a rectangular region. It first selects points on the input contour in virtual space corresponding to uniformly distributed points on the contour of rectangle in physical space. The internal grid is generated by taking these points as boundary conditions and solving the 2D Laplacian equation. The detail of the solution is presented in [4].

Equations (15) and (16) are used to compute material permittivity and permeability tensors for generic transformation. Under the following assumptions, the expression for these quantities can be simplified[5].

- TE or TM mode of propagation.

- Grid lines are orthogonal.
- Size of mesh elements is equal (square mesh).
- Isotropic medium in virtual space.

Under such assumptions, permittivity and permeability in physical space will be simplified as:

- For TE mode of propagation:
  - Constant permeability: $\mu_r(x, y) = \mu_r$.
  - Isotropic permittivity computed as ratio of the area of the cells of the transformation grid.
- For TM mode of propagation:
  - Constant permittivity: $\epsilon_r(x, y) = \epsilon_r$.
  - Isotropic permeability computed as ratio of the area of the cells of the transformation grid.

2.2 Grid Orthogonality Assessment

Since the orthogonality of the transformation grid is the basis for isotropic approximation, it is quantified as follows. Figure 1 shows a sample grid intersection in the complex plane.

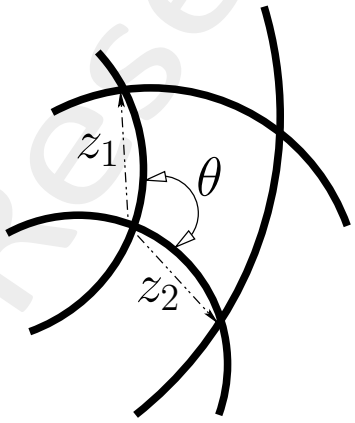

Figure 1. Description of grid orthogonality measure: A sample unit cell of a grid in the complex plane.

Refering to Figure 1, and using Euler's notation, $z_1 = |z_1| e^{j[arg(z_1)]}$, $z_2 = |z_2| e^{j[arg(z_2)]}$, the internal angle θ can be computed as

$$\theta = arg(z_1) - arg(z_2) = arg\left(\frac{z_1}{z_2}\right).$$

The offset from orthogonality χ can then be evaluated as

$$\chi = \theta - 90 \tag{29}$$

3 Numerical Results

3.1 Circular to Linear Array Transformation

Goal: To demonstrate Transformation of an array using the transformation library, and To verify results using full wave simulation.

Test Case Description

The transformation is described pictorially in Figure 1. Figure 1(a) shows the setup of the virtual array under investigation. The region included with the solid curve (Figure 1(a)) is transformed to a rectangular region in the physical space (Figure 1(b)). As a result, the radiating elements that are located on circular contour in the virtual space will be projected to a linear geometry in the physical space. The shaded region in the physical space (Figure 1(b)) shows the location of metamaterial lens.

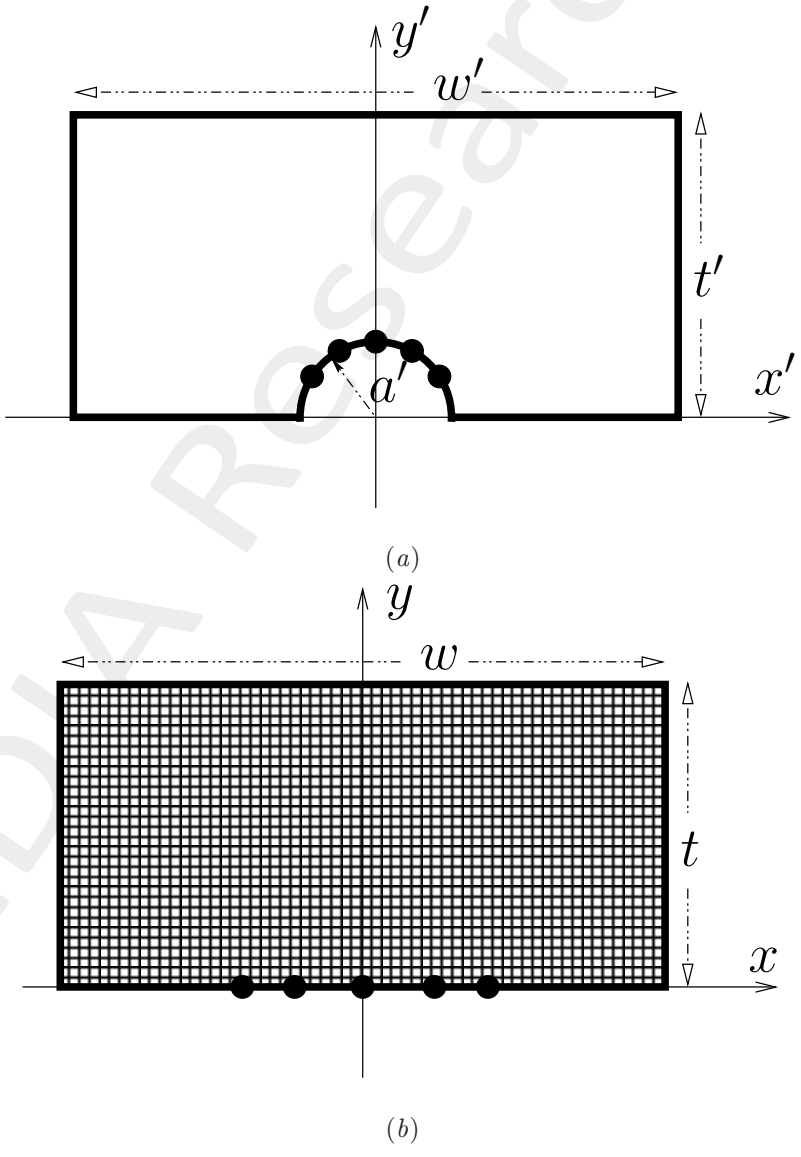

Figure 1. Description of (a) Virtual and (b) Physical spaces.

In the virtual space (Figure 1(a)), a traditional circular array is used and the medium is empty space. The sources in virtual space are uniformly distributed along the circumference of the circle while the physical array has linear distribution.

Simulation Parameters

- Array of Isotropic radiators.
- Number of Array Elements: $N = 9$.
- Frequency of operation: $\nu = 600MHz$
- Wavelength in free space: $\lambda = 0.5m$

Virtual Object Parameters:

- Circular Array of point sources in 2D.
- Radius of the circle: $a' = 2\lambda = 1m$.
- Width of transformation region: $w' = 16\lambda = 8m$.
- Height of transformation region: $t' = 8\lambda = 4m$.
- Element Spacing: $d' = 0.5\lambda = 0.25m$. (Measured along the circumference.)
- Uniform Amplitude Excitation: $I'_n = 1$.
- Pattern steered to $\phi'_s = 30^0$ with phase excitation defined as[6]:

$$\varphi'_n = \frac{-2\pi}{\lambda} a' \cos\left(\phi'_s - \phi'_n\right). \tag{30}$$

  where ϕ'_n is the angular position of the n^{th} radiating element.

Transformation Parameters:

- Number of grid lines along $x' - axis$: $xgrid = 201$.

Full wave simulation Parameters:

- Two dimensional problem.
- TE waves.

There are some differences between the test case presented here and the one presented in the reference paper. The reference paper uses magnetic currents having length of $\frac{\lambda}{40}$ as sources, however, in the test case presented in this report ideal point sources in 2D space are used. Another difference is, in the reference paper, a ground plane is used on one side of the geometry; in contrast scattering boundary conditions are used in all sides of the geometry of the problem presented in this report.

RESULTS

Transformation Grid

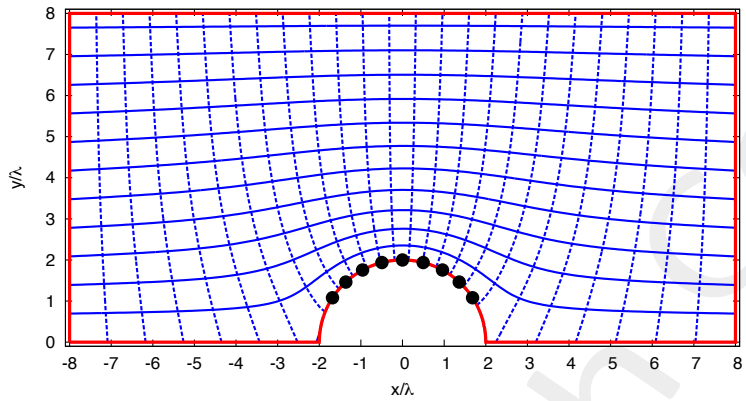

(a)

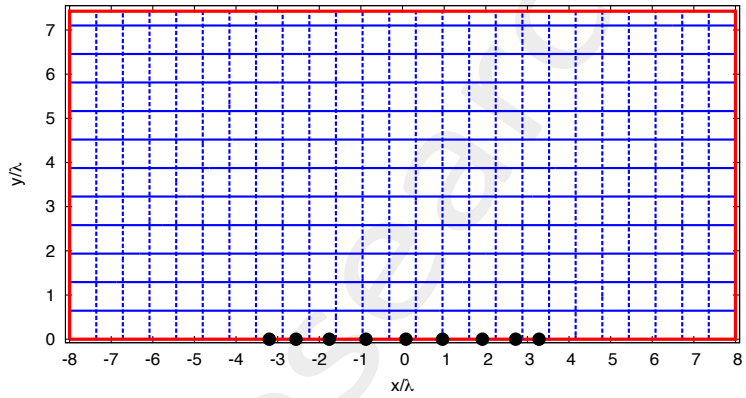

(b)

Figure 2. Transformation Grids: (a) Virtual Space and (b) Physical space.

Observations:

- Number of horizontal grid lines obtained(including the boundaries): $ygrid = 93$.
- The metamaterial lens is discretized into 92×200 cells.
- Each cell has dimensions: $0.08\lambda \times 0.08\lambda$.
- As a result the dimension of the transformation region in physical space is: $w = 200 \times 0.08\lambda = 16\lambda$, $t = 92 \times 0.08\lambda = 7.36\lambda$.

RESULTS

Grid orthogonality assessment.

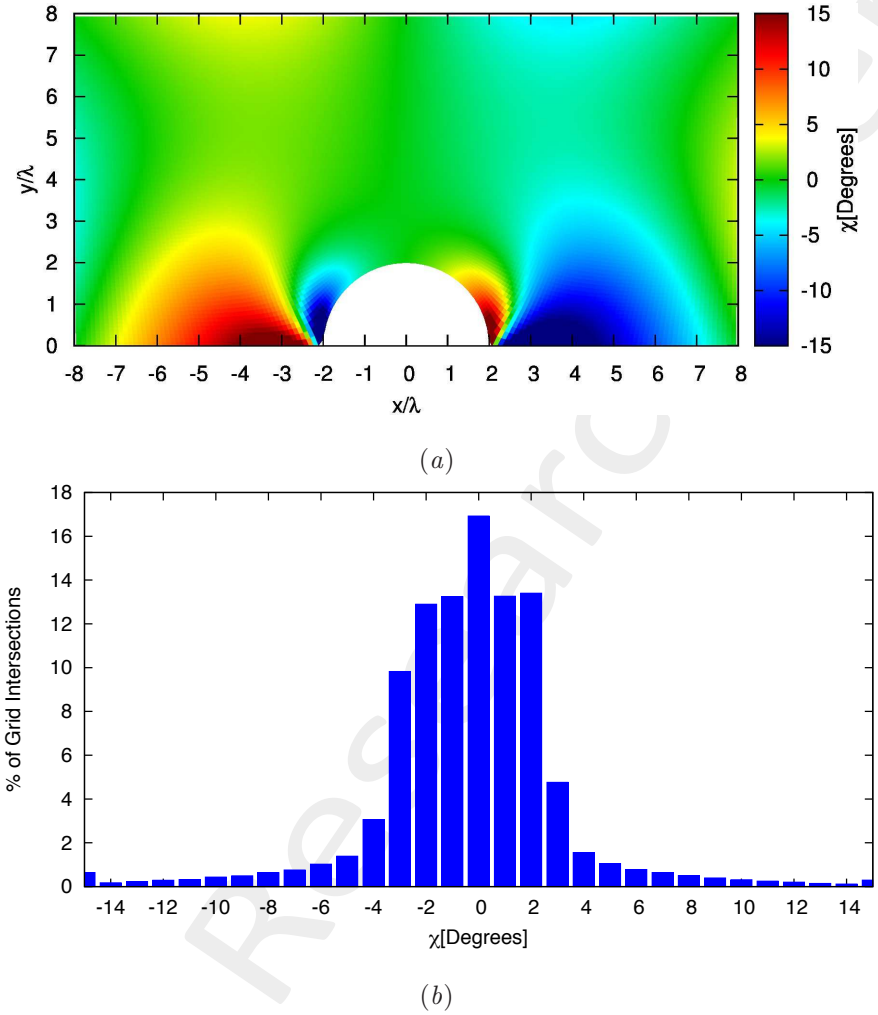

(*a*)

(*b*)

Figure 3. Transformation grid orthogonality test.

Observations:

- Some degree of offset from orthogonality is observed.
- The offset is severe around the transition region from circular to linear. (Figure 3(a)).

RESULTS

Exact values of permittivity.

Because of the two dimensionality of the problem, some of the parameters related to the $z-axis$ are zero valued (i.e $\epsilon'_{vz} = \epsilon_{vz} = \epsilon'_{zv} = \epsilon_{zv} = \mu'_{vz} = \mu_{vz} = \mu'_{zv} = \mu_{zv} = 0$ where $v \in \{x, y\}$). The non-zero valued parameters are reported next.

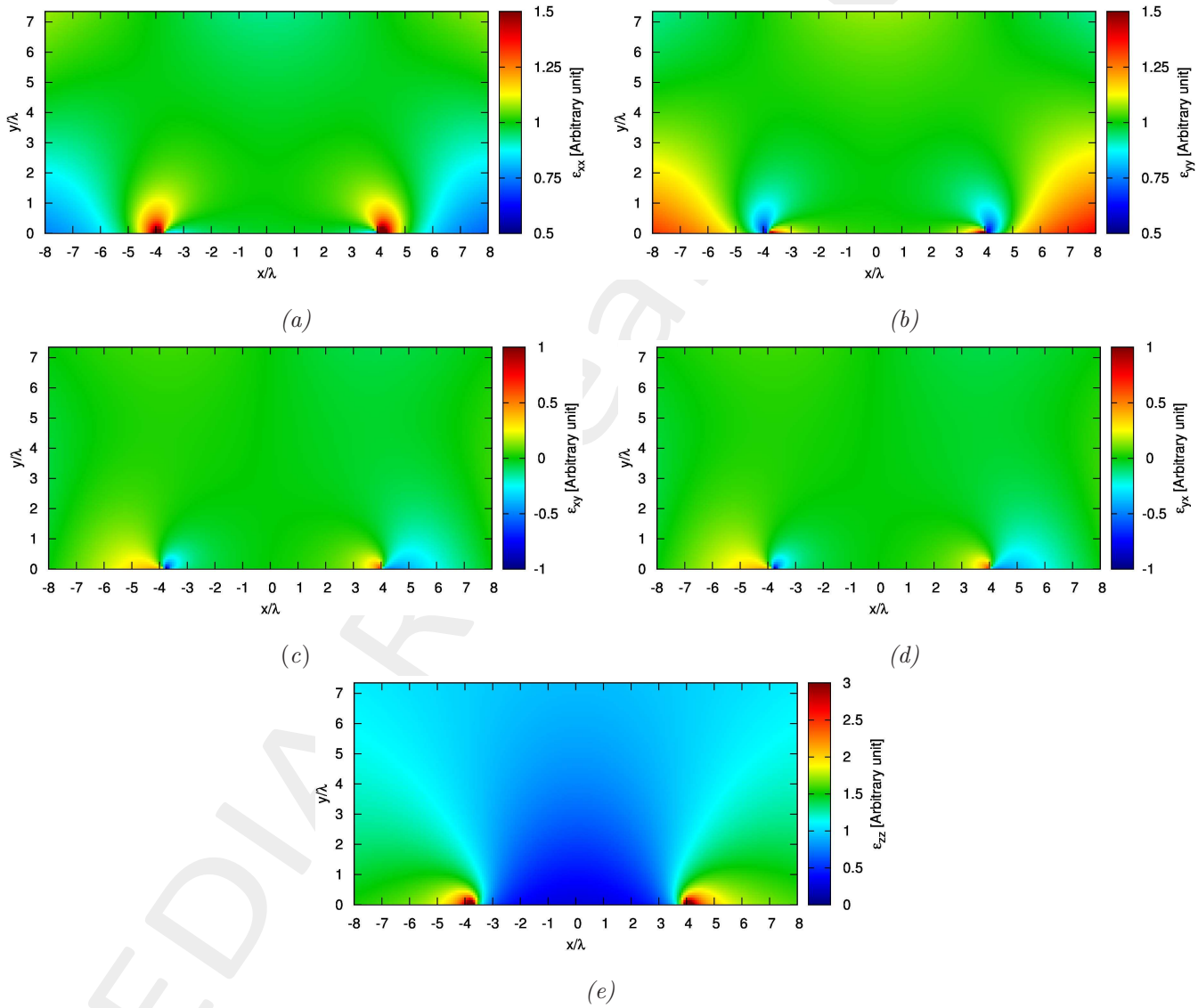

Figure 4. Components of the permittivity tensor in the physical medium.

Observations:

- As expected off-diagonal entries have near zero values at almost all parts of the region: Figures 4*(c)*, 4*(d)*.
- Diagonal entries are near unity: Figures 4*(a)*, 4*(b)*.
- Since the virtual medium is free space ($\epsilon_r' = \mu_r' = 1$), the permeability tensor in the physical medium, $\underline{\mu}$ is the same as that of permittivity, i.e $\underline{\mu} = \underline{\epsilon}$.
- For TE waves, the components of $\underline{\epsilon}$ and $\underline{\mu}$ that contribute are ϵ_{zz}, μ_{xx}, μ_{xy}, μ_{yy} and μ_{yx}.
- The quantities $\mu_{xy} = \epsilon_{xy}$ and $\mu_{yx} = \epsilon_{yx}$ are near zero whereas $\mu_{xx} = \epsilon_{xx}$ and $\mu_{yy} = \epsilon_{yy}$ are near unity.
- As a result, pure Isotropic approximation can be made for TE waves.

RESULTS

Isotropic approximation

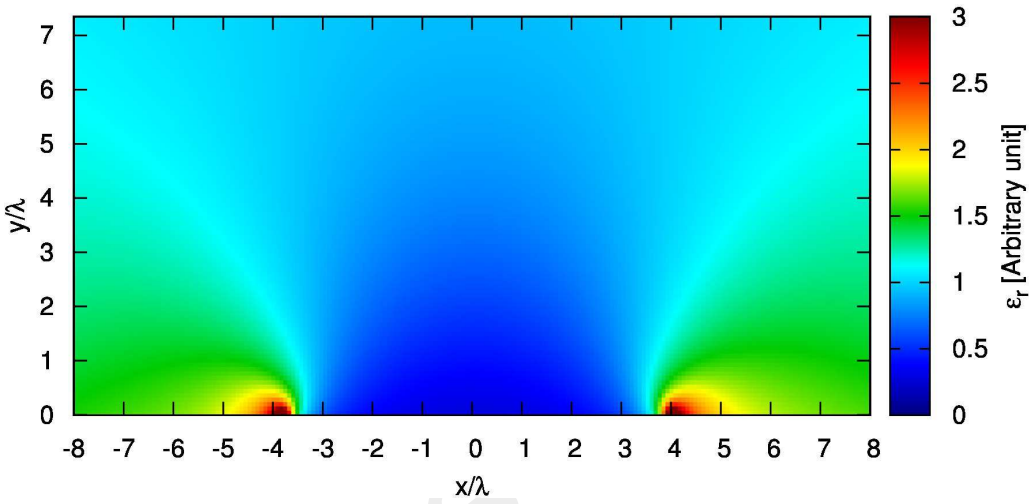

Figure 5. Isotropic permittivity (ϵ_r) of the physical medium computed as ratio of area of transformation grid.

Observations:

- For TE waves, this Isotropic gradient of permittivity (ϵ_r) is used.
- Values are bounded: $0.2680 \leq \epsilon_r \leq 5.8178$.

RESULTS

Simulation Results

The following results report the output of full-wave simulation performed assuming isotropic approximation. The simulation setup considers 2D, TE mode hence, the perpendicular component of the electric field (E_z) is reported. The beam steering direction ($\phi_s = 30^0$) is shown by a broken line.

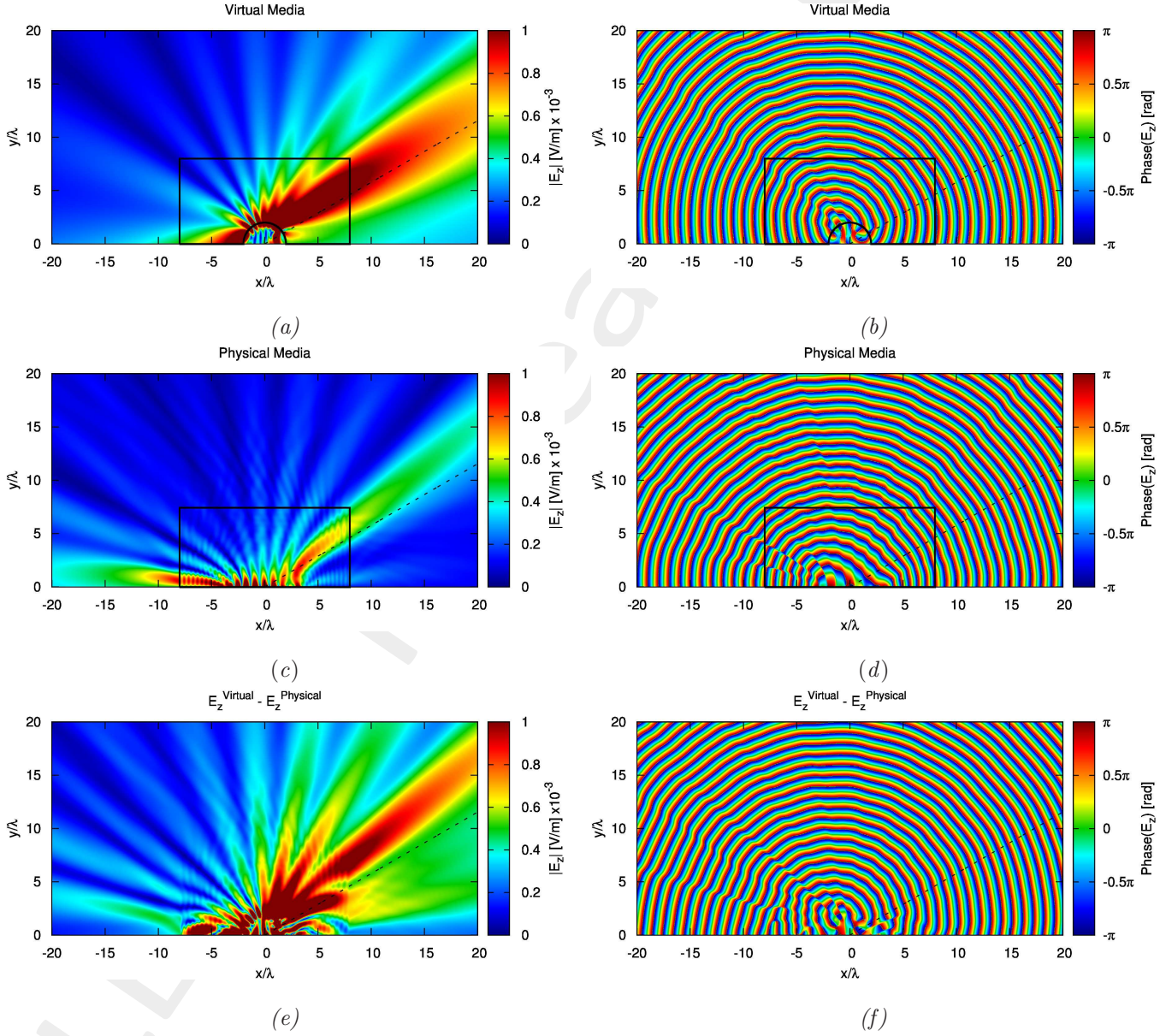

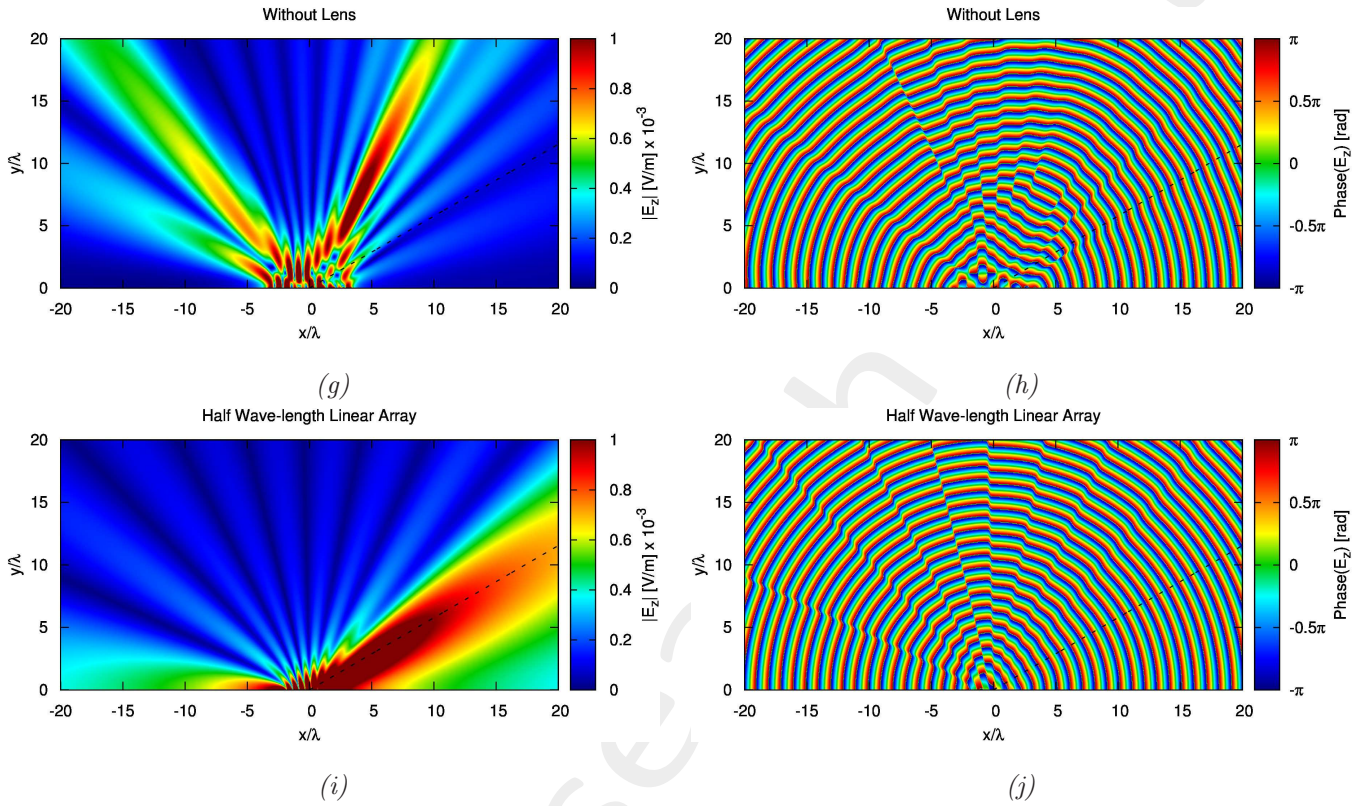

Figure 6. Normal component of the electric field for (a) Virtual Uniform circular array, (b) Ordinary uniform half wavelength array , (c) Transformed linear array, (d) Transformed linear array in the absence of the metamaterial lens.

Observations:

- The transformed linear array along with the lens is is able to steer the beam to wards the expected direction $\phi_s = 30^0$ (Figure 6(c), Figure 6(d)).
- The amplitude the field in the transformed array is considerably smaller than that of the virtual and half wavelength arrays (Figure 6(e), Figure 6(f)).

RESULTS

Comparison of power patterns

The patterns are obtained from COMSOL far-field computing tool.

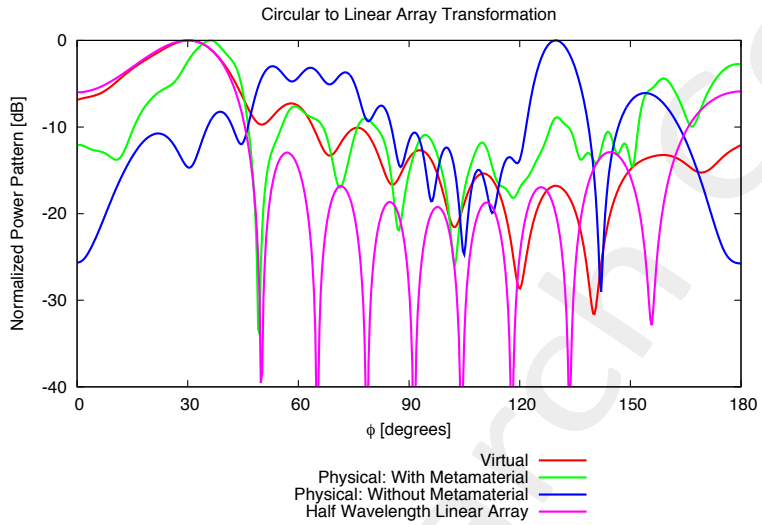

(*a*)

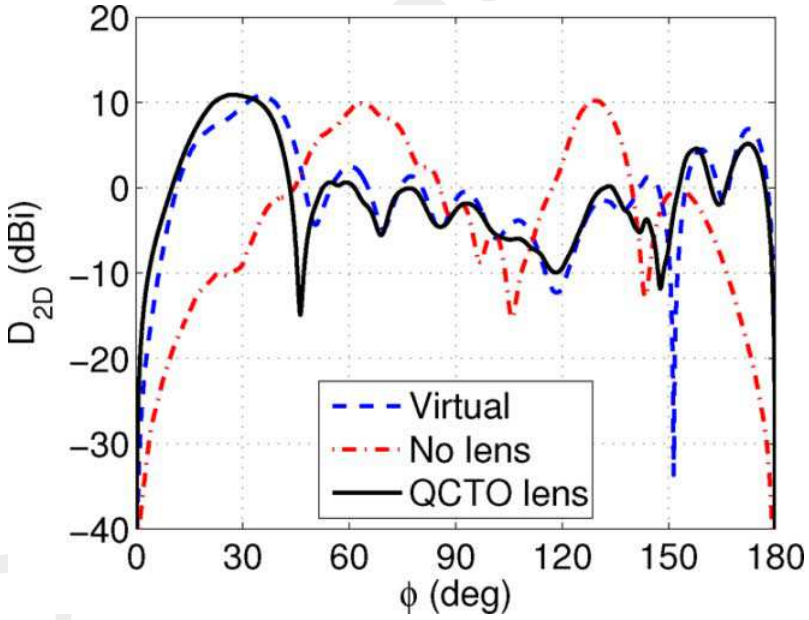

(*b*)

Figure 7. Comparison between normalized power patterns (a) simulation results and (b) from Kwon.2012[1].

RESULTS

Comparison of power patterns

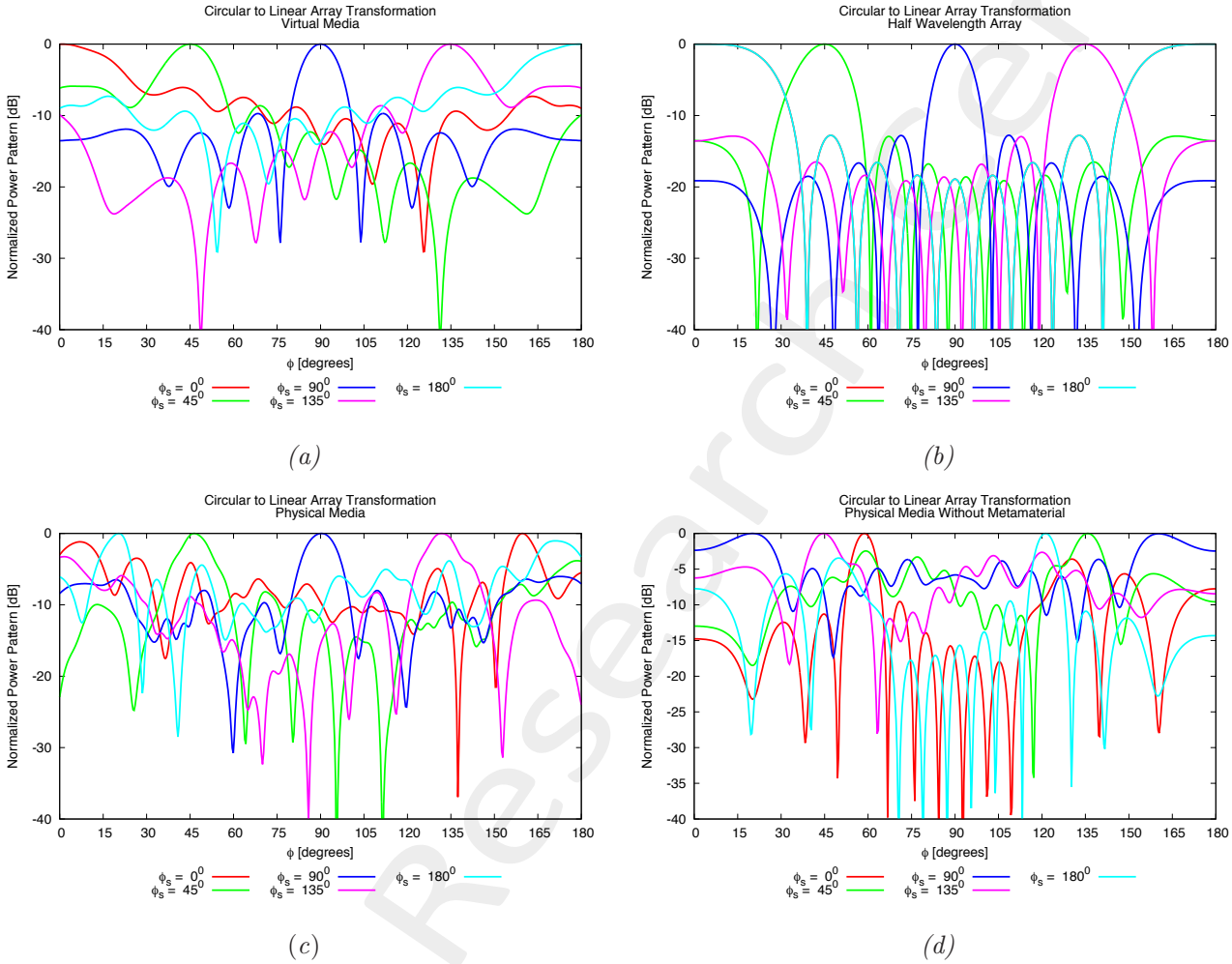

(a) *(b)* *(c)* *(d)*

Figure 8. Plots of normalized power patterns at different steering angles: (a) Virtual circular array, (b) Transformed physical array, (c) Half-wavelength linear array, (d) Transformed physical array without metamaterial.

Observations:

- The shape of the main beam of the linear array with metamaterial lens approximates the semicircular virtual array(Figure 8(c)).
- When the metamaterial medium is removed, the pattern deteriorates (Figure 8(d)).

Comparison of power patterns: 3dB Beam Width

The $3dB$ beam width of the the patterns of Figure 8 are reported here.

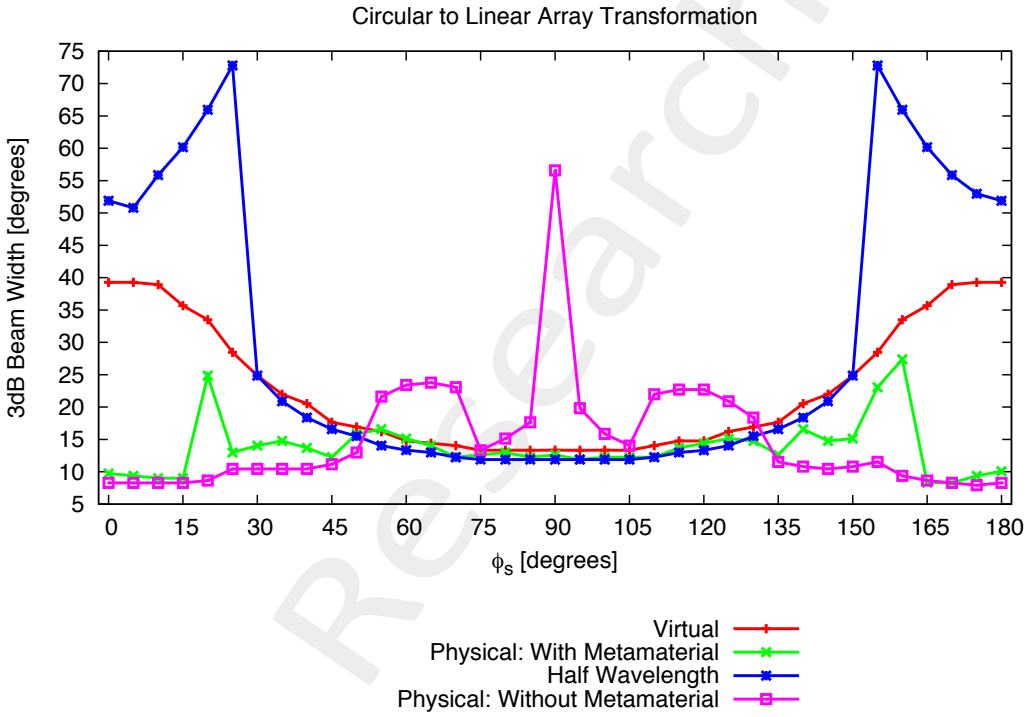

Figure 9. Comparison between normalized power patterns: Plot of beam width at different steering angles.

Acknowledgment

This work has been developed within the EMERALD Project funded by Autonomous Province of Trento - Calls for proposal “Team 2011”.

References

[1] D.-H. Kwon, “Quasi-conformal transformation optics lenses for conformal arrays,” *IEEE Antennas Wireless Propag. Lett.*, vol. 11, pp. 1125-1128, Sept. 2012.

[2] S. A. Cummer, N. Kundtz, and B.-I. Popa, “Electromagnetic surface and line sources under coordinate transformations,” Physical Review Letters A, 80 033820, pp. 033820 1-7, Sept. 2009.

[3] Y. Luo, J. Zhang, L. Ran, H. Chen, and J. A. Kong, “New concept conformal antennas utilizing metamaterial and transformation optics,” IEEE Antennas Wireless Propag. Lett., vol. 7, pp. 509-512, Jul. 2008.

[4] D. C. Ives and R. M. Zacharias, “Conformal mapping and orthogonal grid generation,” *In AIAA/SAE/ASME/ASEE 23rd Joint Propulsion Conference*, San Diego, California, Paper number 87-2057, June 1989.

[5] W. Tang, C. Argyropoulos, E. Kallos, W. Song and Y. Hao, “Discrete coordinate transformation for designing all-dielectric flat antennas,” *IEEE Trans. Antennas Propag.*, vol. 58, no. 12, pp. 3795-3804, Dec. 2010.

[6] C. A. Balanis, *Antenna Theory: Analysis and Design* (3rd Ed.). Wiley, 2005.

[7] P. Rocca, M. Benedetti, M. Donelli, D. Franceschini, and A. Massa, "Evolutionary optimization as applied to inverse problems," Inverse Problems - 25th Year Special Issue of Inverse Problems, Invited Topical Review, vol. 25, pp. 1-41, Dec. 2009.

[8] P. Rocca, G. Oliveri, and A. Massa, "Differential Evolution as applied to electromagnetics," IEEE Antennas and Propagation Magazine, vol.53, no. 1, pp. 38-49, Feb. 2011.

[9] G. Oliveri and A. Massa, "GA-Enhanced ADS-based approach for array thinning," IET Microwaves, Antennas & Propagation , vol. 5, no. 3, pp. 305-315, 2011.

[10] G. Oliveri, F. Caramanica, and A. Massa, "Hybrid ADS-based techniques for radio astronomy array design," IEEE Transactions on Antennas and Propagation - Special Issue on "Antennas for Next Generation Radio Telescopes," vol. 59, no. 6, pp. 1817-1827, Jun. 2011.

[11] L. Poli, P. Rocca, G. Oliveri, and A. Massa, "Harmonic beamforming in time-modulated linear arrays," IEEE Transactions on Antennas and Propagation, vol. 59, no. 7, pp. 2538-2545, Jul. 2011.

[12] L. Poli, P. Rocca, L. Manica, and A. Massa, "Handling sideband radiations in time-modulated arrays through particle swarm optimization," IEEE Transactions on Antennas and Propagation, vol. 58, no. 4, pp. 1408-1411, Apr. 2010.

[13] L. Poli, P. Rocca, L. Manica, and A. Massa, "Time modulated planar arrays - Analysis and optimization of the sideband radiations," IET Microwaves, Antennas & Propagation, vol. 4, no. 9, pp. 1165-1171, 2010.

[14] L. Lizzi, F. Viani, R. Azaro, and A. Massa, "Optimization of a spline-shaped UWB antenna by PSO," IEEE Antennas and Wireless Propagation Letters, vol. 6, pp. 182-185, 2007.

[15] L. Lizzi, F. Viani, R. Azaro, and A. Massa, "A PSO-driven spline-based shaping approach for ultra-wideband (UWB) antenna synthesis," IEEE Transactions on Antennas and Propagation, vol. 56, no. 8, pp. 2613-2621, Aug. 2008.

[16] P. Rocca, L. Manica, and A. Massa, "An improved excitation matching method based on an ant colony optimization for suboptimal-free clustering in sum-difference compromise synthesis," IEEE Transactions on Antennas and Propagation, vol. 57, no. 8, pp. 2297-2306, Aug. 2009.

[17] P. Rocca, L. Manica, and A. Massa, "Ant colony based hybrid approach for optimal compromise sum-difference patterns synthesis," Microwave and Optical Technology Letters, vol. 52, no. 1, pp. 128-132, Jan. 2010.

[18] P. Rocca, L. Manica, F. Stringari, and A. Massa, "Ant colony optimization for tree-searching based synthesis of monopulse array antenna," Electronics Letters, vol. 44, no. 13, pp. 783-785, Jun. 19, 2008.

[19] G. Oliveri and L. Poli, "Optimal sub-arraying of compromise planar arrays through an innovative ACO-weighted procedure," Progress in Electromagnetic Research, vol. 109, pp. 279-299, 2010.

[20] G. Oliveri, "Improving the reliability of frequency domain simulators in the presence of homogeneous metamaterials - A preliminary numerical assessment," Progress In Electromagnetics Research, vol. 122, pp. 497-518, 2012.

[21] I. Martinez, A. H. Panaretos, D. Werner, G. Oliveri, and A. Massa "Ultra-thin reconfigurable electromagnetic metasurface absorbers," 2013 European Conference on Antennas and Propagation (EUCAP), (Gothenburg, Sweden), 8-12 April 2013.

[22] G. Oliveri, P. Rocca, D. H. Werner, E. Bekele, M. Salucci, and A. Massa, "Design and synthesis of innovative metamaterial-enhanced arrays" 2013 IEEE Antennas and Propagation Society International Symposium, (Orlando, USA), July 7-13, 2013.

[23] E. Martini, G. M. Sardi, P. Rocca, G. Oliveri, A. Massa, and S. Maci "Optimization of metamaterial WAIM for planar arrays", 2013 USNC-URSI National Radio Science Meeting, (Orlando, USA), July 7-13, 2013.